

Localization in light nuclei

P.-G. Reinhard,¹ J. A. Maruhn,² A. S. Umar,³ and V. E. Oberacker³

¹*Institut für Theoretische Physik, Universität Erlangen, D-91054 Erlangen, Germany*

²*Institut für Theoretische Physik, Goethe-Universität, D-60438 Frankfurt am Main, Germany*

³*Department of Physics and Astronomy, Vanderbilt University, Nashville, Tennessee 37235, USA*

(Dated: October 5, 2018)

We investigate the presence of spatial localization in nuclei using a method that maps the nucleon same-spin pair probability and is based on the density-matrix. The method is used to study spatial localization of light nuclei within the Hartree-Fock approximation. We show that the method provides an alternative tool for studying spatial localization in comparison to the localization observed from the nuclear mass density.

PACS numbers: 21.60.-n, 21.60.Jz, 21.30.Fe, 21.60.Cs, 27.20.+n, 27.30.+t1

Clustering phenomena in light nuclei have always been an intriguing aspect of nuclear structure physics. Theoretical understanding of why and how conglomeration of nucleons to subunits within a nucleus results in an increase in stability remains an actively investigated question. In particular, alpha clustering in light nuclei has a long history [1–4] and suggests the existence of configurations resembling the formation of *nuclear molecules* [5–7]. It has also been suggested that neutron rich isotopes of some light nuclei may give rise to new types of cluster structures [7, 8]. Most of the theoretical analyses for the cluster structures have been performed with the *a priori* initialization in terms of clusters and effective interactions, which are determined such as to reproduce the binding energies and scattering phase shifts of these configurations. On the other hand, nuclear structure calculations based on the independent-particle approximation or density functionals also manifest cluster-like substructures in the visualization of the total nuclear mass density. For example, Hartree-Fock (HF) calculations for light nuclei often show such formations [9], however since the HF single-particle states are generally spread across the whole nucleus they are delocalized, which makes the identification of these substructures in terms of the single-particle orbitals very difficult. Furthermore, the identification of cluster and shell structures based only on the mass density may be an oversimplification since other aspects of the many-body system, for example the kinetic energy density or density gradients, may help to provide a more detailed understanding of localization. Finally, with the rising popularity of the density functional approach in nuclear physics it may be desirable to have a new localization measure that stems directly from the nuclear density-matrix, since all of the information is contained in this quantity.

An alternative measure of localization had been developed in the context of a mean-field description for electronic systems [10]. A fermionic mean-field state is fully

characterized by the one-body density-matrix

$$\rho_{q\sigma\sigma'}(\mathbf{r}, \mathbf{r}') = \sum_{\alpha \in q} \phi_{\alpha}(\mathbf{r}\sigma) \phi_{\alpha}^*(\mathbf{r}'\sigma'). \quad (1)$$

The probability of finding two nucleons with the same spin at spatial locations \mathbf{r} and \mathbf{r}' (same-spin pair probability) for isospin q is given by

$$P_{q\sigma}(\mathbf{r}, \mathbf{r}') = \rho_{q\sigma}(\mathbf{r})\rho_{q\sigma}(\mathbf{r}') - |\rho_{q\sigma\sigma}(\mathbf{r}, \mathbf{r}')|^2, \quad (2)$$

where $\rho_{q\sigma}(\mathbf{r}) = \rho_{q\sigma\sigma}(\mathbf{r}, \mathbf{r})$ is the local density. The conditional probability for finding a nucleon at \mathbf{r}' when we know with certainty that another nucleon with the same spin and isospin is at \mathbf{r} is

$$R_{q\sigma}(\mathbf{r}, \mathbf{r}') = \rho_{q\sigma}(\mathbf{r}') - \frac{|\rho_{q\sigma\sigma}(\mathbf{r}, \mathbf{r}')|^2}{\rho_{q\sigma}(\mathbf{r})}. \quad (3)$$

Since we are interested in the localization aspects of this probability it is sufficient to consider only the local short-range behavior of the conditional probability, which one can obtain by performing a spherical averaging over a shell of radius δ about the point \mathbf{r} and then Taylor expanding the resulting expression to get [10]

$$R_{q\sigma}(\mathbf{r}, s) \approx \frac{1}{3} \left(\tau_{q\sigma} - \frac{1}{4} \frac{[\nabla \rho_{q\sigma}]^2}{\rho_{q\sigma}} - \frac{\mathbf{j}_{q\sigma}^2}{\rho_{q\sigma}} \right) \delta^2 + \mathcal{O}(\delta^3), \quad (4)$$

where $\tau_{q\sigma}$ and $\mathbf{j}_{q\sigma}$ are the kinetic energy density and current density given by

$$\begin{aligned} \tau_{q\sigma}(\mathbf{r}) &= \sum_{\alpha \in q} |\nabla \phi_{\alpha}(\mathbf{r}\sigma)|^2 \\ \mathbf{j}_{q\sigma}(\mathbf{r}) &= \sum_{\alpha \in q} \text{Im} [\phi_{\alpha}^*(\mathbf{r}\sigma) \nabla \phi_{\alpha}(\mathbf{r}\sigma)] \\ \nabla \rho_{q\sigma}(\mathbf{r}) &= 2 \sum_{\alpha \in q} \text{Re} [\phi_{\alpha}^*(\mathbf{r}\sigma) \nabla \phi_{\alpha}(\mathbf{r}\sigma)]. \end{aligned}$$

The reason for writing $\nabla \rho_{q\sigma}$ explicitly is to emphasize that to have a smooth behavior of the quantities calculated below it is essential to calculate all quantities directly from the wavefunctions. The expression shown in

Eq. (4) suggests the definition of a measure

$$D_{q\sigma}(\mathbf{r}) = \left(\tau_{q\sigma} - \frac{1}{4} \frac{[\nabla \rho_{q\sigma}]^2}{\rho_{q\sigma}} - \frac{\mathbf{j}_{q\sigma}^2}{\rho_{q\sigma}} \right), \quad (5)$$

which is also valid for time-dependent Slater determinants [11]. It is important to remember that $D_{q\sigma}$ is the short-range limit of the conditional same-spin *pair* probability and may contain correlations that are not evident in ordinary one-body observables, such as the mass density. The measure defined by Eq. (5) is a reverse relation, e.g. the larger the probability of finding two same-spin particles in vicinity of each other the smaller the value of D . For this reason it is customary to define a reversed and normalized *localization* measure

$$C_{q\sigma}(\mathbf{r}) = \left[1 + \left(\frac{\tau_{q\sigma} \rho_{q\sigma} - \frac{1}{4} [\nabla \rho_{q\sigma}]^2 - \mathbf{j}_{q\sigma}^2}{\rho_{q\sigma} \tau_{q\sigma}^{\text{TF}}} \right)^2 \right]^{-1} \quad (6)$$

$$\tau_{q\sigma}^{\text{TF}} = \frac{3}{5} (6\pi^2)^{2/3} \rho_{q\sigma}^{5/3},$$

where $\tau_{q\sigma}^{\text{TF}}$ is the Thomas-Fermi kinetic energy density. The current density vanishes in the static case which we will consider in the following. The extreme case of ideal metallic bonding is realized for homogeneous matter where $\tau = \tau_{q\sigma}^{\text{TF}}$. This yields $C = \frac{1}{2}$, a value which thus signals a region with a nearly homogeneous Fermi gas as it is typical for metal electrons, nuclear matter or neutron stars. The opposite regime are space regions where exactly one wavefunction of type $q\sigma$ contributes. This is called *localization* in molecular physics. Such a situation yields $\tau_{q\sigma} \rho_{q\sigma} - \frac{1}{4} [\nabla \rho_{q\sigma}]^2 = 0$ and consequently $C = 1$, the value which signals *localization*. In the nuclear case, it is the α particle which is perfectly localized in this sense, i.e. which has $C = 1$ everywhere. Well bound nuclei are usually metallic and should show predominantly $C = \frac{1}{2}$. Light nuclei are often expected to contain pronounced α -particle sub-structures. These should show up as regions with $C = 1$.

In our calculations, the static HF equations are solved on a Cartesian three-dimensional mesh without any symmetry assumptions. The grid spacing was 1 fm with a box size of $(-15.5, +15.5)$ fm in each dimension. The Skyrme energy functional was employed with the parameterization SkI3 [12]. The spatial derivatives are calculated using the fast Fourier transform and periodic boundary conditions are employed, except for the Coulomb potential, which is calculated with boundary conditions at infinity as described in Ref. [13]. Fig. 1 shows an x - z -cut of the localization function (6) for even-even $N = Z$ nuclei from $A = 4$ to $A = 20$. The left panel shows the proton localization criterion $C_{p\uparrow}$ complemented in the right panel by the corresponding total density. Since the states are spin symmetric, it makes no difference whether we show spin-up, spin-down, or the sum of the two in the localization plots. Similarly, for light $N = Z$ nuclei the isospin

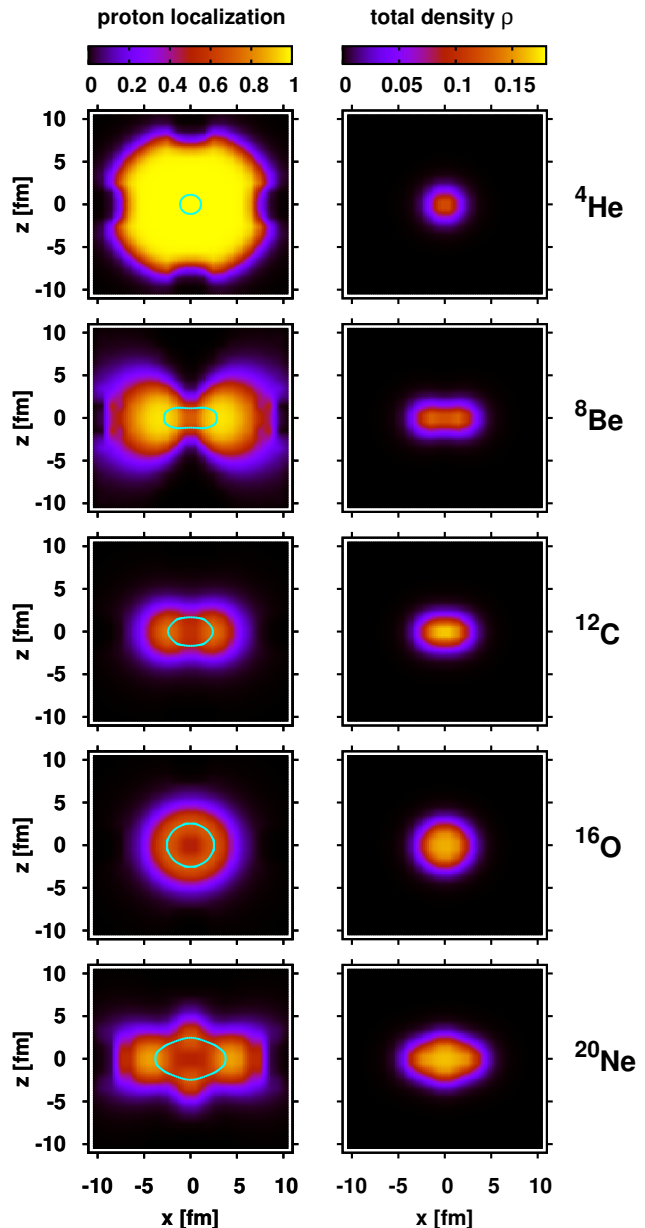


FIG. 1. (Color online) Color map (gray scale) plots of proton localization (left column) and total density in fm^{-3} (right column), for the $Z = N$ nuclei up to ^{20}Ne . The position of the density contour at half nuclear matter density ($\rho = 0.08 \text{ fm}^{-3}$) is indicated with color cyan (light gray) in the maps of proton localization.

dependence of the localization plots are very similar due to the small Coulomb interaction. For neutron rich isotopes this is no longer true as we will show below. The color (gray scale) coding is shown on top of each column and remains the same throughout the column. The position of the density contour at half nuclear matter density ($\rho = 0.08 \text{ fm}^{-3}$) is indicated with color cyan in the maps of proton localization. One should keep in mind that the

maxima and minima of the total nuclear density need not be correlated with that of the localization function, which is a topological quantity to describe localization. The top panel of Fig. 1 shows the calculations for the ${}^4\text{He}$ nucleus. As we have described previously we see a perfect localization with $\mathcal{C} = 1$ in all relevant regions where $\rho > 10^{-4} \text{ fm}^{-3}$. Smaller densities lead to erroneous results for \mathcal{C} due to the very subtle cancellations required. The strongly prolate ${}^8\text{Be}$ shows very distinct localization pattern with perfect localization in the left and right halves of the contour plane and much smaller localization in the contact region where the wavefunctions overlap. As can be seen this is much more pronounced in comparison to the total mass density plot. With this version of the Skyrme force the ground state of ${}^{12}\text{C}$ is oblate deformed as shown in the right pane of Fig. 1. One may be tempted to consider this as a planar arrangement of three α particles. A slight indication of that may be spotted in the localization plot. But it is not well developed, the configuration is too compact, and shows preferably metallic binding. The strongly bound ${}^{16}\text{O}$ nucleus mostly

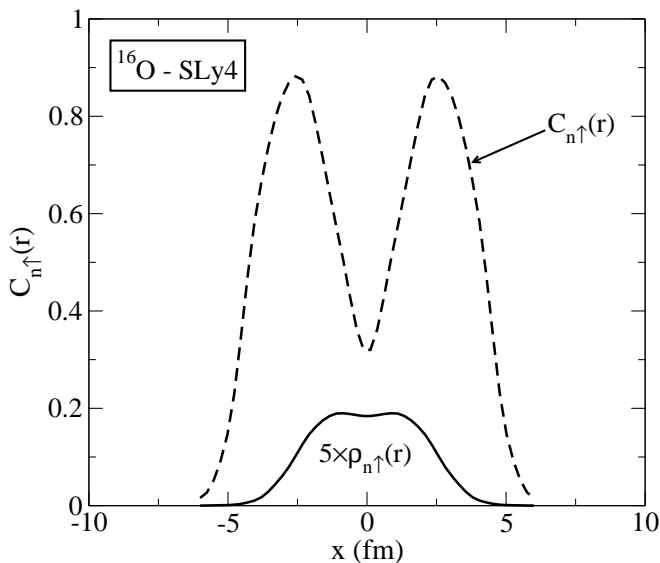


FIG. 2. (Color online) Density profile and localization function for the ${}^{16}\text{O}$ nucleus.

shows a localization value of $\mathcal{C} = \frac{1}{2}$ throughout as one would have expected. The density is known to have a dip at the center [14]. This cannot be discriminated in the density plot here but can be observed as a region of lower localization in the localization map plot. To examine this further we have repeated the same calculation for ${}^{16}\text{O}$ using the SLy4 interaction [15]. In Fig. 2 we show a cut through the profile of the density versus the localization function. We observe that while the central dip in the total density is barely visible the localization function shows a very pronounced dip. Finally, the last panel of Fig. 1 shows results for the strongly prolate ${}^{20}\text{Ne}$ nucleus. The localization map shows two regions of high

localization at the outer ends and a ring of somewhat enhanced localization at the center around the elongation axis. One can interpret this as a quasi-molecular α - ${}^{12}\text{C}$ - α configuration. The α substructures on both sides are almost as well developed as in ${}^8\text{Be}$. We have also computed the further series of $N = Z$ nuclei, ${}^{24}\text{Mg}$, ${}^{28}\text{Si}$, ${}^{32}\text{S}$, ${}^{36}\text{Ar}$, and ${}^{40}\text{Ca}$. These nuclei are increasingly compact and all show basically metallic binding similar to ${}^{12}\text{C}$ and ${}^{16}\text{O}$ shown here.

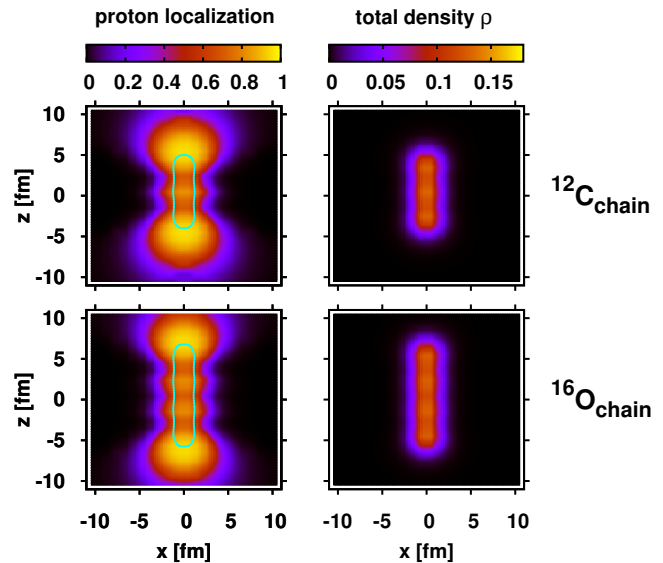


FIG. 3. (Color online) As figure 1, but for chain-like isomers of ${}^{12}\text{C}$ and ${}^{16}\text{O}$.

We have also calculated the isomeric configurations of a number of nuclei. Fig. 3 shows the total density and localization plots for the linear-chain states of ${}^{12}\text{C}$ and ${}^{16}\text{O}$ nuclei. For both the density suggests an α -chain structure which is, indeed, corroborated by the localization that also shows three or four clearly separated maxima, $\mathcal{C} \approx 1$. The region of high localization is very large at both ends, but much smaller for the maxima in the interior due to larger wavefunction overlap. One interesting point about the ${}^{12}\text{C}$ linear-chain configuration localization plot is that in studying the dynamical formation of this chain state, as it was done in Ref. [16], we have observed that the dynamical vibrations of the mass density resembled the localization plot with only the equilibrium shape having the triple- α structure. This is consistent with the kinetic interpretation of the localization function, suggesting that kinetic energies of the same-spin pairs peak mostly around the ends of the linear-chain.

Fig. 4 shows strongly prolate (not yet chain-like isomers which lie higher in energy) isomers of ${}^{24}\text{Mg}$ and ${}^{28}\text{Si}$. Unlike the compact ground-state configurations these isomers indicate interesting molecular substructures. One may interpret ${}^{24}\text{Mg}$ as a α - ${}^{12}\text{C}$ - α molecule and ${}^{28}\text{Si}$ as α - α - ${}^{12}\text{C}$ - α . Again, the outermost α 's are best devel-

oped with large regions of high localization. The inner α 's have already degraded localization due to neighboring wavefunctions from both sides.

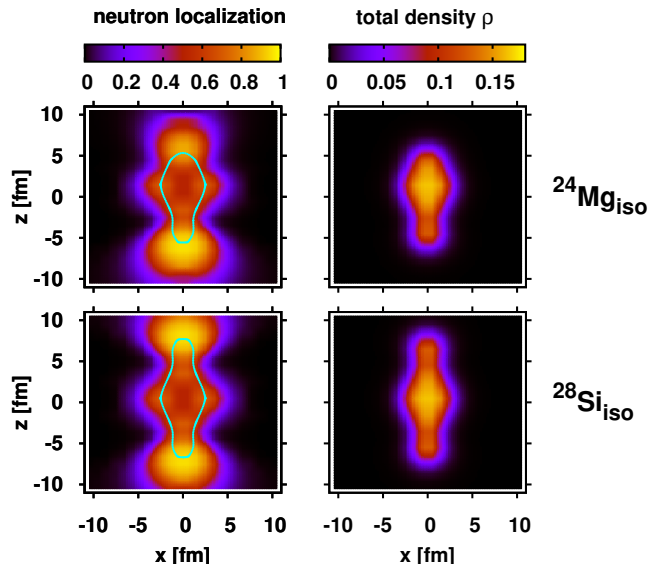


FIG. 4. (Color online) As figure 1, but for stretched isomers of ^{24}Mg and ^{28}Si .

Recently, much interest has been devoted to the study of cluster configurations for neutron-rich isotopes of light nuclei [5, 6, 17]. In particular the linear-chain configurations of C isotopes and their stability against bending modes has been of interest. In Fig. 5 we show both the proton and neutron localization plots for the linear-chain isomer of the ^{20}C nucleus. Due to the neutron richness of ^{20}C the localization plots for neutrons and protons look considerably different. The protons show more distinct regions with high localization value in comparison to the neutron case, which is somewhat diluted due to the large number of neutrons. It is also interesting to observe that the total mass density does not show as clear features as the localization plots.

In summary, we have studied an alternate form of localization measure, which is obtained directly from the density-matrix, in the Hartree-Fock approximation. The localization function depends on kinetic energy density and current density, in addition to the mass density. It can be easily implemented for density functional theory calculations of nuclear structure as well as for time-dependent calculations. One of the fundamental reasons why the new localization measure is such an excellent predictor of correlation and localization is due to the fact that it incorporates the kinetic energy of the relative motion of spin-parallel nucleons at a particular point in space in addition to the mass density for the system [18]. In most cases this localization function shows more detailed localization or clustering features in comparison

to the total mass density. Results for $N = Z$ nuclei up to ^{40}Ca show that pronounced localization, associated with α -particle substructures, appear only for the strongly prolate ^8Be , ^{20}Ne , and of course trivially for ^4He . All other nuclei are more compact and show metallic binding. However, stretched isomers often show convincing α structures, particularly well developed for the α chains of ^{12}C and ^{16}O , but also for the ^{24}Mg and ^{28}Si isomers. In the future we also plan to study the new localization function in time-dependent HF calculations of systems related to nuclear molecular configurations.

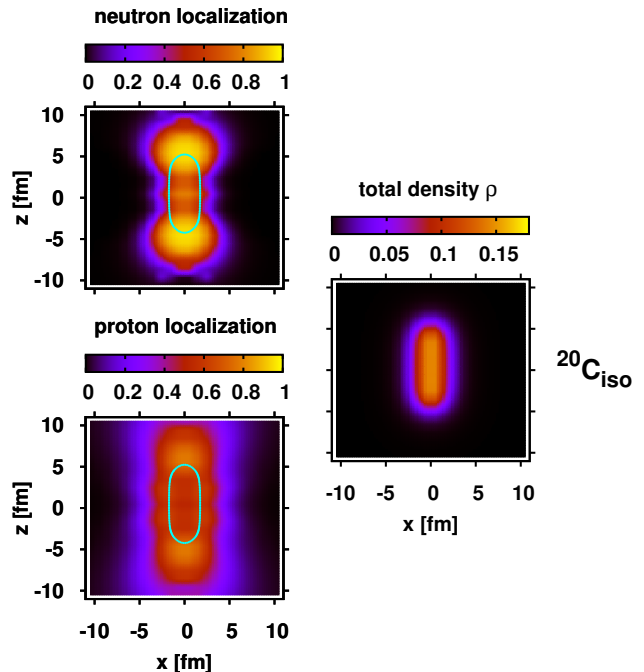


FIG. 5. Color map plots of proton and neutron localization (left column) and total density (right column, density in fm^{-3}) for linear-chain configurations of ^{20}C . The position of the density contour at half nuclear matter density ($\rho = 0.08 \text{ fm}^{-3}$) is indicated with color cyan (light gray) in the maps of localization.

This work has been supported by the U.S. Department of Energy under grant No. DE-FG02-96ER40963 with Vanderbilt University, and by the German BMBF under contract Nos. 06FY9086 and 06ER9063.

-
- [1] L. R. Hafstad and E. Teller, Phys. Rev. **54**, 681 (1938).
 - [2] H. Morinaga, Phys. Rev. **101**, 254 (1956).
 - [3] K. Ikeda, N. Tagikawa, and H. Horiuchi, Prog. Theo. Phys. Suppl., extra number, 464 (1968).
 - [4] D. M. Brink and A. Weiguny, Nucl. Phys. A **120**, 59 (1968).

- [5] N. Itagaki and S. Okabe, K. Ikeda, and I. Tanihata, Phys. Rev. C **64**, 014301 (2001).
- [6] N. Itagaki, W. von Oertzen, and S. Okabe, Phys. Rev. C **74**, 067304 (2006).
- [7] W. von Oertzen, Martin Freer, and Yoshiko Kanada-En'yo, Phys. Rep. **432**, 43 (2006).
- [8] M. Ito, N. Itagaki, H. Sakurai and K. Ikeda, Phys. Rev. Lett. **100**, 182502 (2008).
- [9] J. A. Maruhn, N. Loebl, N. Itagaki and M. Kimura, Nucl. Phys. A **833**, 1 (2010).
- [10] A. D. Becke and K. E. Edgecombe, J. Chem. Phys. **92** 5397 (1990).
- [11] T. Burnus, M. A. L. Marques, and E. K. U. Gross, Phys. Rev. A **71**, 010501(R) (2005).
- [12] P.-G. Reinhard and H. Flocard, Nucl. Phys. **A584**, 467 (1995).
- [13] J. W. Eastwood and D. R. K. Brownrigg, J. Comp. Phys. **32**, 24 (1979).
- [14] J. Friedrich and N. Vögler, Nucl. Phys. A **373**, 192 (1982).
- [15] E. Chabanat, P. Bonche, P. Haensel, J. Meyer and R. Schaeffer, Nucl. Phys. **A635**, 231 (1998); **A643**, 441(E) (1998).
- [16] A. S. Umar, J. A. Maruhn, N. Itagaki, and V. E. Oberacker, Phys. Rev. Lett. **104**, 212503 (2010).
- [17] J. A. Maruhn, N. Loebl, A. S. Umar, N. Itagaki, M. Kimura, H. Horiuchi, and A. Tohsaki, Mod. Phys. Lett. A **25**, 1866 (2010).
- [18] J.F. Dobson, J. Chem. Phys. **94**, 4328 (1991).